LA-UR-85-2459

AUG 07 1985

CONF-850706--29

Los Alamos National Laboratory is operated by the University of California for the United States Department of Energy under contract W-7405-ENG-36.

LA-UR--85-2459

DE85 015711

TITLE: REACTION RATES FROM ELECTROMAGNETIC GAUGE DATA

AUTHOR(S): John Vorthman
George Andrews
Jerry Wackerle

SUBMITTED TO: The Eighth Symposium (International) on Detonation

DISCLAIMER

Los Alamos Los Alamos National Laboratory
Los Alamos, New Mexico 87545

FORM NO 836 R4
ST NO 2629 5/81

REACTION RATES FROM ELECTROMAGNETIC G.." E DATA

John Vorthman, George Andrews, and Jerry Wackerle
Los Alamos National Laboratory
Los Alamos NM 87544

The determination of reaction rates in explosives from experimental data is a task that requires a great deal of care, patience, and curve fitting. We have found that by measuring more quantities than are mathematically necessary for a complete Lagrange analysis, curve fits to experimental data do not have to be as exacting as otherwise required. We present an experimental technique specifically designed for the determination of global reaction rates which uses both embedded electromagnetic impulse and particle velocity gauges. The methods used to efficiently analyze the data, and the results and conclusions reached from several such studies are also presented.

INTRODUCTION

The determination of global reaction rates from embedded-gauge data has been a modest, but continuing effort at Los Alamos for nearly a decade [1-4]. Other laboratories have had similar efforts [5-7]. The usual procedure is to conduct one-dimensional experiments to measure, in a sufficiently reacting explosive, the pressure-field history, p(h,t), or particle-velocity-field history, u(h,t), or both, over as large a Lagrangian distance-time (h,t) region as practical. These data are then treated with a so-called Lagrange analysis, integrating the conservation relations for momentum, mass and energy:

$$\frac{\partial u}{\partial t} = -\frac{1}{\rho_o}\frac{\partial p}{\partial h} \quad , \qquad (1)$$

$$\frac{\partial (1/\rho)}{\partial t} = \frac{1}{\rho_o}\frac{\partial u}{\partial h} \quad , \qquad (2),$$

and

$$\frac{\partial e}{\partial t} = -p\frac{\partial (1/\rho)}{\partial t} = -\frac{p}{\rho_o}\frac{\partial u}{\partial h} \quad , \qquad (3)$$

to determine the density- and energy-field histories, $\rho(h,t)$ and $e(h,t)$. With these fields known, an assumed reactant-product equation of state, $p(\rho,e,\lambda)$ or $e(p,\rho,\lambda)$ allows calculation of the global reaction progress field, here specified by the mass fraction of products, $\lambda(h,t)$. The time derivative of this variable determines a reaction rate, $r = \partial\lambda/\partial t$, which can be correlated to the other state variables to postulate, evaluate and calibrate "rate laws" for the explosive.

In this paper we describe electromagnetic (EM) gauging experiments specifically designed for the determination of reaction rates in shocked explosives. Projectiles from a light-gas gun are used to generate one-dimensional reactive flow in high-explosive target., with impact velocities chosen so that the explosive is building up to, but does not attain, detonation in the distance-time region covered by the measurements. The explosive has a collection of electrical conductors (the EM gauge package) embedded in it and is surrounded by an external magnetic field. The motion of the conductors in the magnetic field generates a collection of voltages that are recorded and later used to determine the pressure- and velocity-field histories that characterize the shock-induced reactive flow in the explosive. The gauge package we presently use allows the measurement of particle velocity and impulse--the time integral of the pressure--at five locations in the explosive. This provides sufficient data to perform the Lagrange analysis and rate determination.

The measurement of both velocity and impulse (with pressure available by time differentiation) histories and the sufficiency of data from a single experiment are two major advantages of our electromagnetic gauge system. The integration of Eqn. (1)-(3) requires the

evaluation of spatial gradients through a few gauge locations. Consequently, Lagrange analysis becomes a considerable exercise in curve fitting. In the earlier work [1-3,5], only pressure measurements were acquired, so that the calculated density- and energy-field histories effectively depend on the curvatures of the functions fitted through the data. With the new system, single applications of first-order spatial derivatives suffice for all of the analysis. Investigations using only pressure data required combining results from several different shot experiments, and small shot-to-shot variations in loading conditions and reaction histories added difficulty to the analyses. The new system has some potential for further miniaturization and has less problems with electrical breakdown of gauge insulation than encountered with Manganin pressure gauges.

ANALYSIS OF THE GAUGE RESPONSE

The development of electromagnetic particle-velocity gauges for shock-dynamic measurements is over two decades old [8], and provided the first in-material gauging of any kind in reacting explosives [9]. The usual design is sketched in Fig. 1-a. When a shock has traveled from the projectile-target interface past the line bc, the wire segment bc will be moving with the local particle velocity of the target material. Faraday's law gives

$$V = -\frac{d}{dt}\int \vec{B}\cdot d\vec{S}$$

for the voltage, V, produced in the wire, where $\vec{B}$ represents the magnetic field (taken to be uniform and constant in the laboratory, or Eulerian, reference frame), and the surface integral includes the changing area, S, inside the wire loop. Call x' the Eulerian coordinate of the wire segment bc and ℓ the constant length of the segment bc. Then, if $\vec{B}$ is perpendicular to the plane of the gauge,

$$V = -\ell B \frac{d}{dt}\int_{x'}^{R} dx = \ell B u \quad , \quad (4)$$

where u is the velocity of the wire segment bc. Thus a knowledge of the magnetic field, the length of the active element of the gauge ℓ, and the voltage produced allows one to determine the particle velocity of the target at a Lagrangian position inside the material.

Although the ability to use an EM gauge to find pressure was recognized some time ago [10], this method is

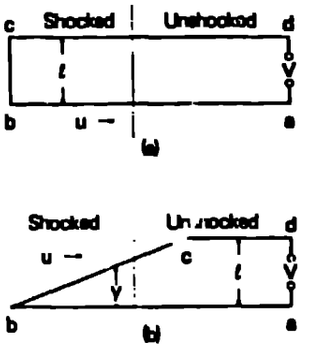

Fig. 1 - Electromagnetic Gauges.
(a) Velocity gauge, (b) Impulse gauge.

neither widely known nor used. Pressure can be found with the experimental configuration shown in Fig. 1-b and a slightly more complicated analysis than that used above. With the Eulerian-Lagrangian transformation $\rho\, dx = \rho_o\, dh$, Faraday's law gives

$$V = -B\frac{d}{dt}\int_b^c y(h)\,\frac{\rho_o}{\rho}\,dh$$

$$= -B\frac{d}{dt}\int_b^c \tan\theta\,(h-b)\,\frac{\rho_o}{\rho}\,dh$$

$$= -B\,\rho_o \tan\theta \int_b^c (h-b)\,\frac{\partial(1/\rho)}{\partial t}\,dh \ ,$$

where $\tan\theta$ is the initial slope of the wire and we restrict the analysis to times before the shock arrives at c. Substituting in the equation for mass conservation, Eq. (2), and integrating by parts, gives

$$V = -B\tan\theta\int_b^c (h-b)\,\frac{\partial u}{\partial h}\,dh$$

$$= -B\tan\theta\left[\,(h-b)\,u\,\right]_b^c - \int_b^c u\,dh\,\right) \ .$$

Noting that $u(c,t) = 0$, one has

$$V = B\tan\theta\int_b^c u\,dh \ . \qquad (5)$$

In our usual situation, each mass point experiences a shock discontinuity followed by continuous motion. Consequently, the particle velocity in the field spanned by the gauge can be written:

$$u(h,t) = u_1 + \int_{t_1}^{t}\frac{\partial u}{\partial t}\,dt' \ ,$$

where $u_1(h)$ is the particle velocity behind the shock and $t_1(h)$ the shock arrival time, both depending on the distance coordinate alone. Use of momentum conservation, Eq. (1), and transfer of the spatial derivative to outside the integral give:

$$u(h,t) = u_1 - \frac{1}{\rho_o} \int_{t_1}^{t} \frac{\partial p}{\partial h}\, dt' \quad ,$$

$$= u_1 - \frac{1}{\rho_o} \left(\frac{\partial}{\partial h} \int_{t_1}^{t} p\, dt' - p_1 \frac{dt_1}{dh} \right) .$$

Noting that dt_1/dh is just the reciprocal of the shock velocity, U_1, the first and third term of the last equation cancel from the Hugoniot relation, $p_1 = \rho_o u_1 U_1$. Defining the impulse*, $I(h,t)$, as the time integral of the pressure, there results:

$$\rho_o u = - \frac{\partial I}{\partial h} = - \frac{\partial}{\partial h} \int_{t_1}^{t} p\, dt' \quad . \quad (6)$$

With this preparation, evaluating the response of the impulse gauge is simply a matter of substituting Eq. (6) for the particle velocity in Eq. (5). This gives

$$I(b,t) = - \int_{b}^{c} \frac{\partial I}{\partial h}\, dh = \frac{\rho_o V}{B \tan\theta} \quad (7)$$

for the impulse at the apex of the gauge element until the shock reaches point c.

The determination of pressure from the impulse measurement requires some differentiation of data. A simple, if not always best, method is to evaluate the time derivative:

$$p(b,t) = \frac{\partial I}{\partial t} = \frac{\rho_o}{B \tan\theta} \frac{dV}{dt} \quad . \quad (8)$$

If the data have any imperfections, these imperfections will be amplified when pressure is calculated in this manner. More serious, if the data have detailed structure, as in a short-shock experiment, this detail may be difficult to retain accurately through the time differentiation process. An effective alternative for calculating pressure-field histories under such circumstances will be discussed in the section on Lagrange analysis.

*Strictly speaking, I is the impulse per unit area; we will ignore this distinction.

A PRACTICAL DESIGN

In practice, measuring particle velocity and impulse is not as simple as inserting wires into an explosive. As the explosive reacts, care must be taken to assure that the gauge elements move with and not through the gaseous products. In addition, the explosive products are electrically conductive so that gauge leads should be insulated [11]. If, as some workers prefer, particle-velocity gauge leads are brought out of the explosive parallel to the shock front (unlike the gauge shown in Fig. 1), care must be taken to assure that two-dimensional flow does not cause the leads to spread and generate extraneous voltages [12]. The finite width of the gauge leads can also be a problem when trying to measure the distance t (see Fig. 1-a).

The gauge package shown in Fig. 2 was designed to minimize the above problems. Leads are only 100-μm wide and 18-μm thick, and are sandwiched between two 25-μm-thick Teflon sheets. The Teflon coating acts as a mechanical substrate, a barrier to gas flow around the conductors, and as electrical insulation. Aluminum conductors are used because this metal is a relatively good shock impedance match to most explosives. This impedance match minimizes both perturbations to the flow and problems with gauge leads punching through the Teflon sheet.

The gauge package is inserted into the explosive at an angle, as shown in Fig. 3. This gauge insertion technique has the advantage that the explosive need be sliced only once, yet locates each pair of impulse and velocity gauges at different depths in the explosive. We commonly use a gauge package inclined twenty or thirty degrees to the impact

Fig. 2 - The electromagnetic gauge package. The largest velocity gauge is 10-mm wide.

face and 2-mm separation of gauge pairs in the package (see Fig. 2), giving 0.7- or 1-mm spacing of the gauge elements in the direction of particle motion. Gauge leads are brought out through the rear edge of the target and the gauge-package dimensions are limited so that two-dimensional effects caused by edge rarefactions are avoided.

The gauge package and target are assembled by first bonding aluminum foil to a Teflon sheet that has been specially treated to accept the adhesive. The glue bond is kept as thin as possible, typically about 2-μm thick. Next, the conductor pattern shown in Fig. 2 is photo etched from the metal. Gauge construction is completed when the top of the conductors are covered with another Teflon sheet, also bonded in place. Next, the explosive sample is sliced, the gauge package inserted, and the explosive pieces glued together. It is important to keep the gauge-glue combination as thin as possible. If the gauge or glue is too thick, the gauge will not record the bulk response of the explosive. The type of glue used to hold the gauge in the explosive can also affect the response of the gauge. Some glues approved for use with explosives contain solvents that can cause small voids in the explosive near the gauge package. Such glues are to be avoided if the bulk response of the explosive is to be measured.

The uniform magnetic field indicated in Fig. 3 is provided by a specially constructed electromagnet. The two pole pieces for the magnet are 0.28-m square and 0.25-m thick, and have a 0.28-m separation. These pole pieces are designed to be integrated into our gas-gun target chamber, which serves as the yoke and magnetic return path for the system. An aluminum alloy cylinder inside the magnet poles is used to protect it and the target chamber from shrapnel from the target assembly. The magnet pole pieces are each wound with three parallel coils on a 0.1-m iron core, powered by a 15-V, 300-A regulated DC supply. Magnetic field strengths are measured for each experiment, and are typically 825 gauss. A central, 25-mm, cubic region between the poles has been shown to have ± 0.5-percent uniformity in magnetic field, and the gauge package is located within this region for all experiments. Disturbance of the magnetic field by an incoming, conducting projectile was avoided by using the plastic projectile extension and aluminum oxide (chosen for high shock impedance) flyer depicted in Fig. 3.

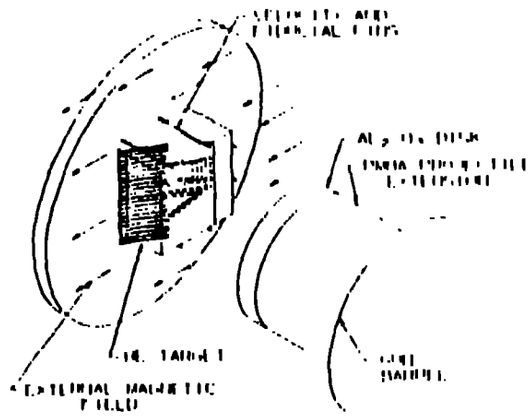

Fig. 3 - Experimental Assembly

The magnetic-field strengths, gauge-element dimensions and particle velocities of our experiments combine to give typical signals of about a volt. These were recorded on Tektronix Model 7844 oscilloscopes or, more recently, Model 7612 transient digitizers. In both cases, the signals are recorded through Model 7A13 and 7A24 amplifiers used in the differential mode. Single ended measurements proved to be impractical because of grounding problems at the gauge.

In this paper, the experimental and analytic methods discussed above are illustrated with two results for PBX 9501, a plastic-bonded, 95 weight percent HMX similar to the PBX 9404 studied previously [2]. Projectile velocities and ceramic flyer thicknesses were chosen to give a 3.5-GPa sustained-shock input for one experiment and a 3.9-GPa, 0.45-μs pulsed input for the other. In both cases, the first gauge-element pair was about 0.3 mm from the impact face; the fifth element was 3 mm from the impact face for the sustained-shock experiment and 4.3-mm deep for the short-shock test. The deepest element pair was less than half of the run distance to detonation for both of the input shock conditions chosen. Impulse and particle-velocity data for the two experiments are shown as frames (a) and (b) in Figs. 4 and 5.

LAGRANGE ANALYSIS

Each of the experiments described above provides enough impulse- and velocity-field data to allow a Lagrange analysis of the reactive flow. As was the case for the analysis of pressure-gauge data only [3], we have found that

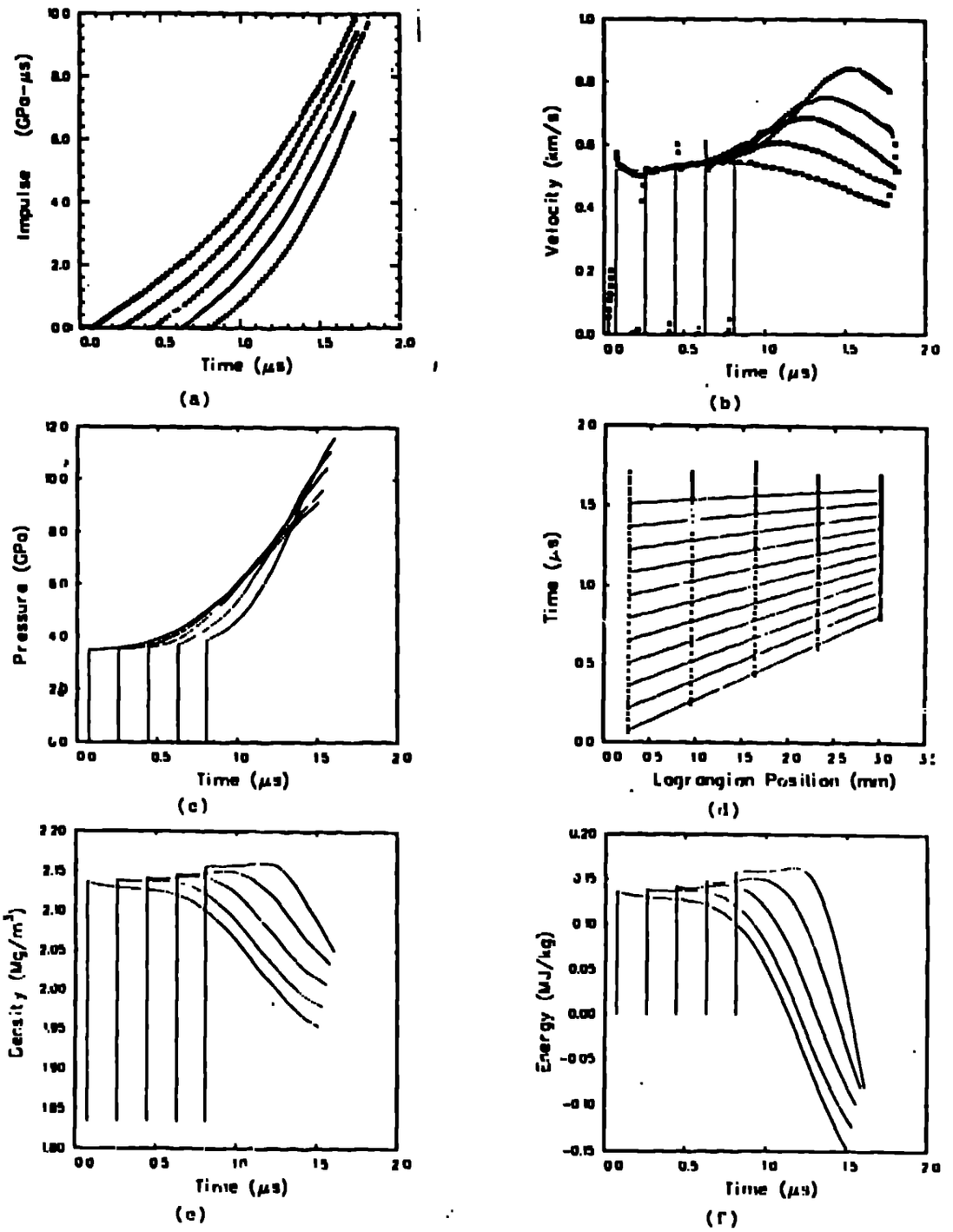

Fig. 4. - State histories for a sustained-shock experiment on PBX 9501. Gauge elements are located 0.27, 0.96, 1.64, 2.32 and 3.01 mm from the impact face.

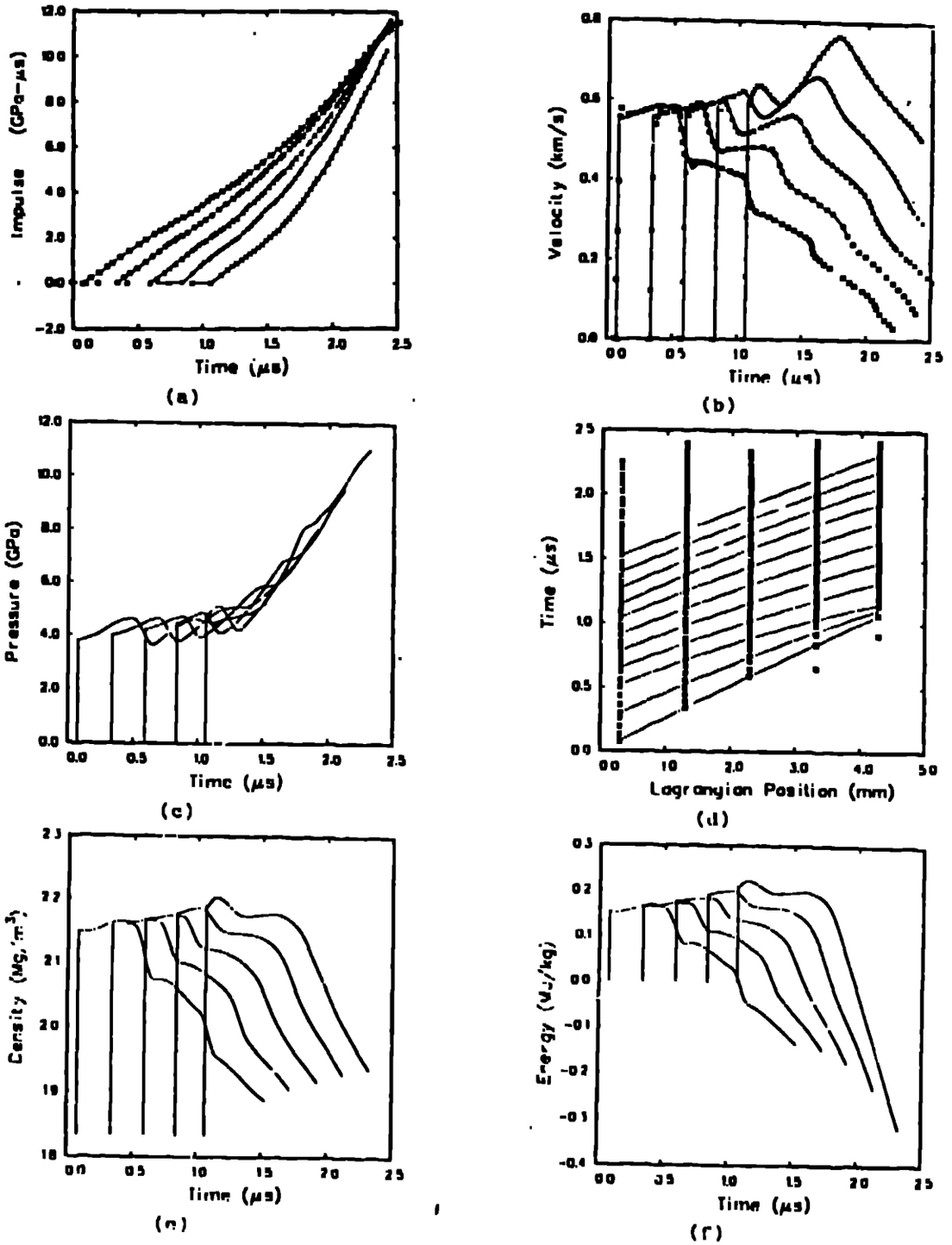

Fig. 5. - State histories for a short-shock experiment on PBX 9501. Gauge elements are located 0.30, 1.10, 2.29, 3.31 and 4.29 mm from the impact face.

the Lagrange analysis of these data is best accomplished using the so-called pathline method[13]. In this analytic technique, the gauge data are fitted along arbitrary paths constructed through the entire h-t space of the observations. The spatial derivatives in Eqs. (1) to (3) are replaced with the directional derivatives, according to the transformation of any state variable, f, by

$$\frac{\partial f}{\partial h} = \frac{df}{dh} - \frac{1}{U}\frac{\partial f}{\partial t} , \qquad (9)$$

where df/dh denotes the derivative along the pathline and U = 1/(dt/dh) is termed the phase velocity. Although this transformation replaces an interpolation through a few gauge locations with the difference in two quantities, this does not lead to a less accurate analysis. The paths are chosen analytically, so no error occurs in U; the $\partial f/\partial t$ are fitted through dense data at each gauge station; finally, the paths can be chosen so that state variables do not change along them as much as at fixed time, so that the df/dh are smoother and more accurately evaluated than the $\partial f/\partial h$.

With the combined impulse and velocity data provided by the EM gauge package, an alternative to time differentiation of the impulse records is allowed by the pathline analysis method. Applying the transformation Eq. (9) to the impulse, and using Eqs. (6) and (8) for its spatial and time derivatives, we have:

$$p(h,t) = \left(\rho_o u + \frac{dI}{dh} \right) U . \qquad (8')$$

Note the resemblance of this expression of the pressure to the Hugoniot relation, with the the phase velocity in the role of a shock velocity; it reduces to the Hugoniot relation on the first pathline, where $I_1 = 0$.

With the pressure-field history defined by Eq. (8) or Eq. (8'), the Lagrange analysis is completed by the integration of mass and energy conservation, Eqs. (2) and (3). Defining the compression, $\eta = 1 - \rho_o/\rho$, these are written:

$$\eta(h,t) = \eta_1(h) - \int_{t_1}^{t} \left(\frac{du}{dh} - \frac{1}{U}\frac{\partial u}{\partial t} \right) dt' \qquad (10)$$

and

$$e(h,t) = e_1(h) - \frac{1}{\rho_o}\int_{t_1}^{t} p \left(\frac{du}{dh} - \frac{1}{U}\frac{\partial u}{\partial t} \right) dt' . \qquad (11)$$

The Lagrange analyses of the two experiments described above had some common features and some important differences. In both cases, the analysis was done with a construction of 101 pathlines. Shock states on the first path line were specified by fitting the initial particle velocities and using the known unreacted Hugoniot for the explosive. Mathematical cubic spline fitting was used to construct smooth functions of the impulse- and velocity-gauge histories; these fitting functions are shown as solid curves in frames (a) and (b) of Figs. 4 and 5. The integration of Eqs. (10) and (11) was accomplished with a simple differencing scheme for both analyses. Our present analysis determines density and energy histories at the gauge locations only.

For the analysis of the sustained-shock data, simple time differentiation of the impulse data was found an adequate means of evaluating the pressure histories. Evaluating the derivatives of the spline fitting functions of Fig. 4-a gave the fairly pleasing result shown in Fig. 4-c. An uncomplicated, regular pathline construction was also found adequate; every tenth pathline of the construction used is shown in Fig. 4-d, with the symbols indicating the extent of the data. Pathline derivatives of the particle velocities, du/dh, were evaluated by cubic spline fitting of five velocity values on each pathline and calculating the derivative at each gauge location. These were combined with the time derivatives of the velocity and impulse fitting functions and the analytic formulations of the phase velocities to compute the density and energy histories according to Eqs. (10) and (11). The results are shown in Fig. 4-e and 4-f and are similar in form and reasonably regular.

Some modification of the analysis is needed to treat short-shock data such as shown in Fig. 5. Although the impulse data of Fig. 5-a show some breaks and kinks associated with the successive rarefactions evident in the velocity data, reasonable pressure histories could not be obtained by simple time differentiation of spline functions fitted to the impulse histories. Consequently, the alternative analysis of pressure histories, Eq. (8'), was used. In order to avoid pathline to pathline irregularity in the U, du/dh and dI/dh factors in Eqs. (8'), (10) and (11), it was necessary to use very low-order, smooth functions for fitting velocity and impulse along the path lines, and for the pathline functions as well. This was accomplished by

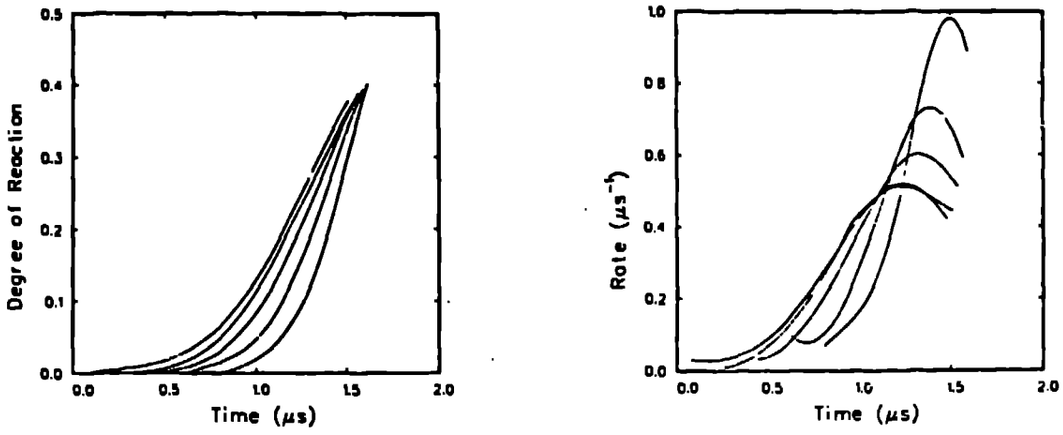

Fig. 6 Reaction and rate histories for sustained-shock experiments.

fitting certain key path lines through the flow features of heads and tails of the rarefaction waves, and spacing the intermediate path lines evenly; the resulting construction is shown in Fig. 5-d. We were able to use single quadratic segments for all fitting functions. The calculated pressures shown in Fig. 5-c have a generally increasing character, with superimposed reverberating rarefaction features synchronized with similar features in the velocity records. The detailed structure of the the pressure histories is primarily due to the $\rho_o u$ term in Eq. (8'), and the dI/dh term provides the increasing character. Similarly, in the calculation of density and energy histories, it is the du/dh term in Eqs. (10) and (11) that determines the general trends and the term with $\partial u/\partial t$ that superimposes the detailed structure. This ability of the experimental design and analysis to connect pressure, density and energy histories all to the particle-velocity histories permits the pleasing results in Fig. 5 and rate analyses for complex reactive flows.

EQUATION OF STATE AND REACTION RATES

Calculation of reaction and rate histories is effected by the assumption of a reactant-product equation of state. We consider the reacting explosive as a mixture of unreacted solid and fully reacted, mostly gaseous products and measure reaction progress in terms of the mass fraction of products, λ. As in most of our previous work, we have used the HOM equation of state [14]. Mie-Grueisen representations are used for both constituents, with the measured Hugoniot serving as the reference curve for the solid and a well-calibrated BKW [14] calculation of the isentrope through the Chapman-Jouguet state references the products. Ideal mixing of specific volume and internal energy are assumed, along with pressure and temperature equilibrium. Our calculation of $\lambda(\rho,p,e)$ is done with a Newton's method iteration algorithm and computer subroutine devised by Charles Forest. The calculation also provides such thermodynamic derivatives as the sound speed, c, and the pressure derivative $p_\lambda = (\partial p/\partial \lambda)_{\rho,e}$. A detailed description of a similar computation is in [15].

Reaction histories calculated with HOM for the two experiments on PBX 9501 are shown in Figs. 6-a and 7-a Both are quite regular. We exercise either of two options in calculating the rates. One is to evaluate time derivatives of pressure and density in the Lagrangian analysis and calculate

$$r = \frac{\partial \lambda}{\partial t} = \frac{(\partial p/\partial t) - c^2(\partial \rho/\partial t)}{p_\lambda} \quad . \quad (12)$$

This was done for the rate histories for the sustained-shock case shown in Fig. 6-b. The other alternative is spline-fitting of the reaction histories and differentiating. This was done for the three interior gauge locations for the short-shock case, Fig. 7-b. The results are more erratic than the sustained-shock case; we have not yet found a really effective fitting method. This was particularly the case for the first and fifth gauge stations, so only results at the central three locations are shown in Fig. 7.

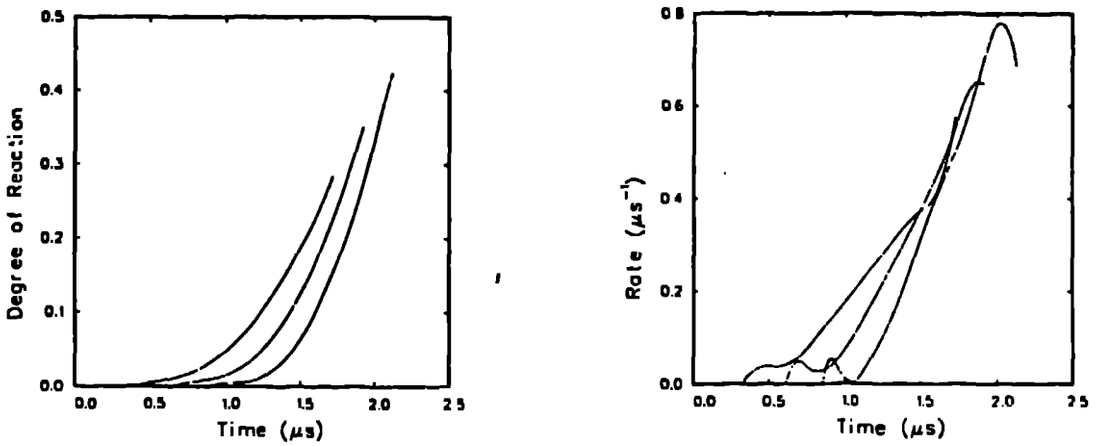

Fig. 7 Reaction and rate histories for short-shock experiments.

EMPIRICAL REACTION-RATE CORRELATIONS

Since our group first attempted to obtain an empirical rate correlation for PBX 9404, we have recognized that a simple dependence on current pressure provided a reasonable correlation for rates analyzed from sustained-shock experiments[2]. However, the same work showed that rates from short-shock experiments failed to correlate with current pressure, and that a larger range of initiation phenomena could be modeled with a reaction-rate dependence combining multiplicative factors in the depletion, shock strength and current state. Our empirical manifestation of the fact has been the Direct Analysis Generated Modified Arrhenius Rate, or DAGMAR. This form provided excellent correlations of rates from both sustained- and short-shock experiments on PBX 9404[2], and subsequently a good rate calibration for 1.8-g/cm³ TATB[3]. Both calibrations have been generally successful in hydrocode simulations of a variety of initiation phenomena, including those in state regions much different from those of the gauge experiments used to determine the rates. This success recently has been extended to detonation reaction zone observations on TATB[16].

The current-pressure correlations of the rates calculated for PBX 9501 are shown in Fig. 8, plotted in a coordinate system appropriate for the usual expression for the Forest Fire rate [14],

$$\ln\left(\frac{r}{1-\lambda}\right) = \sum_{J=0}^{n} a_J \, p^J \quad . \qquad (13)$$

The rate histories for the sustained-shock experiment obviously admit to a current-pressure correlation over most of the $0 < \lambda < 0.4$ reaction range. Because the pressure histories in the short-shock case increase overall during the time covered by experiment (see Fig. 5-c), the correlation is reasonable overall. However, local portions with strongly increasing rates and constant or decreasing pressures are not consistent with Eq. (13). The dashed line is the Forest Fire rate calibrated in the usual manner, using explosive wedge data and a rather assumptive, shock-change analysis of the buildup of the shock front. Although the Forest Fire calibration is by no means a best fit to our rate histories, it is remarkable that it is in the general vicinity, considering the different types of data and analyses used.

The formulation of DAGMAR is:

$$\frac{r}{1-\lambda} = Z_0 \, p_1^n \, G(p,t) \, e^{-(T^*/T)} \quad , \qquad (14)$$

where p_1 is shock-front pressure, T is the current temperature (a parameter of questionable physical significance, calculated in HOM), and Z_0, n and T^* are constants. $G(p,t)$ is an induction-time factor that becomes unity in a few tenths of a microsecond; this was necessary for the PBX 9404 correlation, but not for the 1.8-g/cm³ TATB. On an Arrhenius plot, the function plots as a series of parallel straight lines except as modified by the $G(p,t)$ factor at early times (lower temperatures).

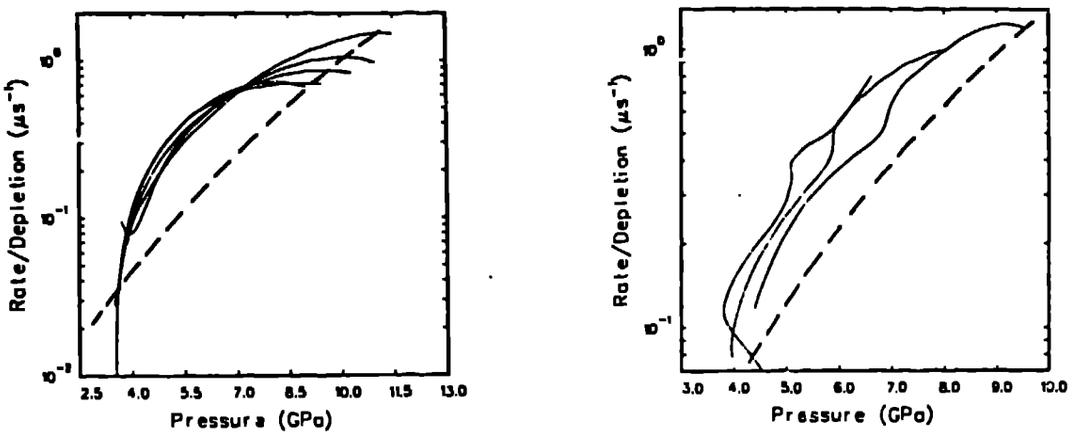

(a) (b)

Fig. 8 - Pressure correlation for (a) sustained- and (b) short shock experiments.

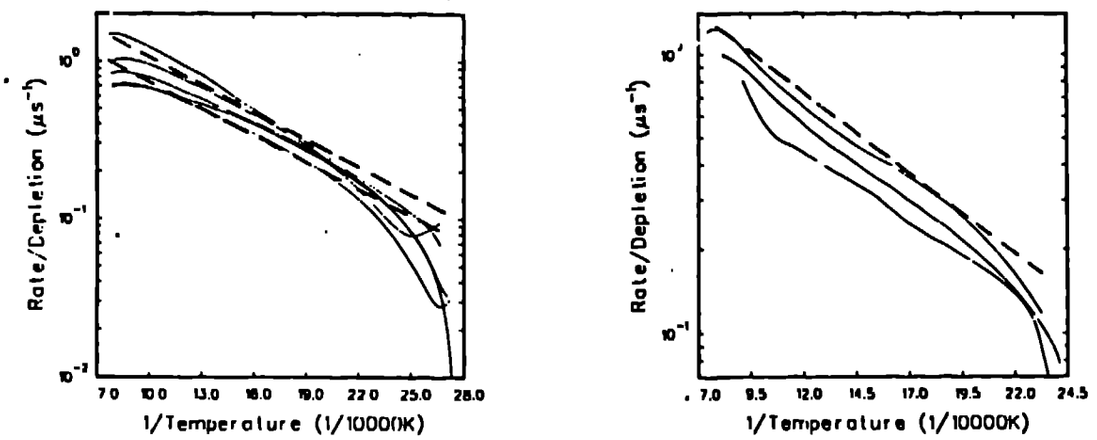

(a) (b)

Fig. 9 - DAGMAR correlation for (a) sustained- and (b) short-shock experiments.

Figure 9 shows that DAGMAR correlates well with our rate data for both sustained- and short-shock experiments on PBX 9501. In both cases, the curves lie at higher levels in sequence of increasing shock strength with deeper gauges. The range of shock pressures in these experiments is not enough to evaluate the exponent n, so we presently use the $n = 2$ for PBX 9404 for this constant. The graphically matched dashed lines in Fig. 5-a correspond to the shock states at the first and last gauges, and represent $T^* = 1260$ K and $Z_0 = 0.205$--a slightly larger rate than for PBX 9404. The same constants are used to plot the rate for the center gauge for the short-shock data; it is a bit high. We have not yet attempted to calculate an induction-time factor, but the rates at early times indicate one is needed for PBX 9501.

Although the short-shock experiment on PBX 9404 made the point better, our intent in displaying the correlations above is to indicate that more can be learned about global reaction rates analyzing such experiments than with sustained-shock data. The Lagrange analyses of the pressure-gauge data for the short-shock experiments on PBX 9404 [2] are recalled by the responsible

author (JW) as a process of lengthy labor and some rather shameful finagling. Anderson substantially improved the analysis of pressure-gauge data for the work on TATB [3], but was unable to accomplish a Lagrange analysis of the short-shock data at all. Although there are several improvements planned for the analysis reported here, it is already relatively little work, free of manipulation, and effective.

The electromagnetic combined impulse and particle-velocity system allows rate analyses of more complex one-dimensional reactive flow. In our group, the hope is to proceed from empirical correlations to more physical reaction-rate models for heterogeneous explosives, and our belief is that the proper way to test and calibrate these models is with global reaction-rate information. For those content with testing and calibrating their models with trial-and-error computer simulations of observations, we recommend embedded-gauge measurements that are less demanding experimentally than those we have described.

REFERENCES

1. Jerry Wackerle, J. O. Johnson, and P. M. Halleck, "Shock Initiation of High Density PETN," Sixth Symposium on Detonation, Office of Naval Research Report ACR-221, p.20, 1976.

2. Jerry Wackerle, R. L. Rabie, M. J. Ginsberg, and A. B. Anderson, "A Shock Initiation Study of PBX 9404," Proceedings of the Symposium on High Dynamic Pressures, Paris, France, p. 127, 1978.

3. Allan B. Anderson, M. J. Ginsberg, W. L. Seitz, and Jerry Wackerle, "Shock Initiation of Porous TATB," Seventh Symposium on Detonation, Office of Naval Research Report MP 82-334, p. 385, 1981.

4. John Vorthman and Jerry Wackerle, "Multiple-Wave Effects on Explosives Decomposition Rates," Proceedings 1983 APS Topical Conference on Shock Waves, p. 613, North-Holland, Amsterdam, 1984.

5. G. I. Kanel and A. N. Dremin, "Decomposition of Cast TNT in Shock Waves," Fizika Goreniya i Vzryva, 13, No. 1, p. 85, 1977.

6. G. L. Nutt and L. M. Erickson, "Reactive Flow Lagrange Analysis in RX-26-AF", Proceedings 1983 APS Topical Conference on Shock Waves, p. 605, North-Holland, Amsterdam, 1984.

7. Jiao Quinjie, Ding Jing, Liang Yunming, Huang Zhengping and Zhao Hengyang, "Hugoniots and Reaction Rates from EMV Gauge Measurements and Lagrange Analysis," This symposium.

8. A. N. Dremin and G. A. Adadurov, "The Behavior of Glass Under Dynamic Loading," Soviet Physics-Solid State, 6, p. 1379, 1964.

9. A. N. Dremin, S. A. Koldunov, "Shock Initiation of Detonation in Cast and Pressed TNT," Vzrivnoe Delo, No. 63/20, p. 37, Moscow, Nedra, 1967.

10. C. Young, R. Fowles, and R. P. Swift, "Shock Waves and the Mechanical Properties of Solids," edited by J. J. Burke and V. Weiss, Syracuse University Press, 1971.

11. B. Hayes, "Electrical Measurements in Reaction Zones of High Explosives," 10th Symposium on Combustion, p. 869, The Combustion Inst., 1965.

12. L. M. Erickson, C. B. Johnson, N. L. Parker, H. C. Vantine, R. C. Weingart, and R. S. Lee, "The Electromagnetic Velocity Gauge: Use of Multiple Gauges, Time Response, and Flow Perturbations," Seventh Symposium on Detonation, Office of Naval Research Repor MP 82-334, p. 1062, 1981.

13. Lynn Seaman, "Lagrangian Analysis for Multiple Stress or Velocity Gages in Attenuating Waves," J. Appl. Phys. 45, No. 10, p. 4303, 1974.

14. Charles L. Mader, "Numerical Modeling of Detonation," University of California Press, Berkeley, 1979.

15. J. N. Johnson, P. K. Tang, and C. A. Forest, "Shock-wave Initiation of Heterogeneous Reactive Solids," J. Appl. Phys. 57, No. 9, p. 4323, 1985.

16. W. L. Seitz, H. L. Stacy, and Jerry Wackerle, "Detonation Reaction Zone Studies on TATB Explosives," this symposium.